Advanced chemical design with supported metal complexes for selective catalysis

Mizuki Tada and Yasuhiro Iwasawa*

Received (in Cambridge, UK) 31st January 2006, Accepted 7th March 2006
First published as an Advance Article on the web 29th March 2006
DOI: 10.1039/b601507g

This review covers several recent topics of novel catalyst design with supported metal complexes on oxide surfaces for selective catalysis such as chiral self-dimerization to create asymmetric oxidative coupling catalysis, surface functionalization with achiral reagents to promote asymmetric catalysis, and molecular imprinting to design shape-selective catalysis. The new concepts and designs find wide applications to a variety of selective catalysts.

1. Introduction

New materials with distinct chemistry prepared stepwise in a controllable manner by using organometallic and inorganic complexes as precursors provide an opportunity for the development of efficient catalytic molecularly-organized surfaces.[1–8] The key factors in the chemical design of supported catalyst surfaces are composition, structure, oxidation state, distribution, morphology, polarity, *etc.*, which should be organized at the surface. Reports on progress in several techniques for *in-situ* characterization of catalyst surfaces have documented dynamic behaviors of supported metal complexes on surfaces and active structures for selective catalysis, and the obtained structural information has provided feedback for new strategies for catalyst design.[8,9] A large store of knowledge of the relationship between active structures and their catalysis allows prediction of the reactivity of supported catalyst surfaces.

The chemical design of catalyst surfaces is now reaching the stage of regulation of selective catalysis for a variety of important chemical products. The control of the coordination of active metal centers has been indispensable for the selective chemical rearrangement of reactant molecules, but their reactivity depends on not only the electronic configuration of metal centers but also their environments on the surface, which regulate the reaction paths and hence the selectivity of catalysis. Comprehensive design and construction of chemical architectures on surfaces provide novel approaches to develop selective catalysis such as asymmetric catalysis which has not been developed successfully in the field of heterogeneous catalysis so far.

However, the chemical design of definite structures and compositions prepared on oxide surfaces are generally still difficult challenges because of a lack of established methods and techniques for synthesis and transformation of active structures at surfaces and characterization of the prepared surface species.[6–8] Heterogeneity of oxide surfaces also

Department of Chemistry, Graduate School of Science, The University of Tokyo, Hongo, Bunkyo-ku, Tokyo, 113-0033, Japan. E-mail: iwasawa@chem.s.u-tokyo.ac.jp; Fax: +81-3-5800-6892; Tel: +81-3-5841-4363

Mizuki Tada

Dr Mizuki Tada was born in 1979 in Tokyo, Japan. She studied in and received her BSc (2001) and MSc (2003) from the Department of Chemistry, Graduate School of Science at The University of Tokyo. She became a JSPS fellow (2003–2005) and received her PhD in 2005 from The University of Tokyo under the supervision of Prof. Yasuhiro Iwasawa. Since 2005, she has been an assistant professor in the Department of Chemistry, Graduate School of Science at The University of Tokyo. Her current research focuses on catalyst surface design with supported metal complexes, molecular imprinting, characterization of catalyst surfaces, and time-resolved XAFS.

Yasuhiro Iwasawa

Prof. Dr Yasuhiro Iwasawa was born in 1946 in Saitama, Japan. He received his BSc (1968), MSc (1970), and PhD (1973) from the Department of Chemistry, Faculty of Science at The University of Tokyo. He moved to Yokohama National University in 1972 as a Research Associate and became Lecturer in 1977, then Associate Professor in 1981. He returned to the Department of Chemistry, The University of Tokyo in 1984 as Associate Professor and became Professor in 1986. His research interests are catalyst surface design, reaction mechanism, in situ characterization of oxide surfaces by SPM, time-resolved XAFS. He has been honored with many awards including the Medal with Purple Ribbon (2003).

prevents researchers from making inroads on the uniform active sites on supported catalyst surfaces. Recently, we have proposed the advanced design of catalyst surfaces managing surfaces as a foundation to mediate regulated architecture as not only a simple support grafting active metal complexes, and have found novel tools toward asymmetric catalysis: surface OH-promoted chiral self-dimerization of Schiff-base complexes[10,11] and achiral surface functionalization enhancing enantioselective catalysis.[12,13] In this review, we introduce some examples of advanced catalyst design with supported metal complexes mediated by surfaces for selective catalysis.

2. Advanced chemical design with supported metal complexes on oxide surfaces

Three novel methods for advanced surface design with supported metal complexes for selective catalysis, which have been developed by us, are illustrated in Fig. 1.

Sharp selectivity can be achieved on metal-complex catalysts, where the regulation by ligands in metal complexes allows selective catalysis and asymmetric synthesis. However, homogeneous metal complexes in solutions are generally easy to gather and can cause undesired decomposition during catalytic cycles, resulting in loss of the catalytic activities. Transformation of homogeneous catalysts to heterogeneous catalysts with molecular-level active structures has been accomplished by attaching metal complexes on oxide supports to provide coordinatively unsaturated and regulated structures on the surfaces as illustrated in Fig. 1.[1–8,14–16] Attaching metal complexes to oxide surfaces provides new catalytic systems that have the advantages of both heterogeneous and homogeneous catalysts. We have discovered a new phenomenon of self-dimerization of metal complexes on oxide surfaces. By using this phenomenon one can create new chiral space around the metal centers for enantioselective reactions as shown in Fig. 1. The supported chiral metal complexes may also be regulated chemically and physically by grafting molecules modifying the surface, resulting in promotion of the chiral property. Advanced catalytic materials can also be designed through the combination of metal-complex attachment and molecular imprinting on oxide surfaces as shown in Fig. 1. The imprinting of metal complexes may be a promising way to design artificial enzymatic catalysts with 100% selectivity for target reactions. The precise characteristics of active structures on surfaces of conventional supported metal catalysts are often difficult to ascertain especially under catalytic reaction conditions despite the progress of *in-situ/operando* techniques, which results in the restriction of the development of new catalytic materials on surfaces. Molecular-level control of catalyst surfaces is necessary for design of multi-functionalized catalytic sites.

3. *Interfacial chemical bonding for catalysis (strategy 1):* Oxide-surface promoted alkene hydrogenation on supported Pd-monomer complexes

A C–N bond formation, hydroamination, is crucial for the synthesis of valuable new amine derivatives, which have been produced *via* several synthetic processes. However, this reaction is generally slightly exothermic and entropically negative,[17] and the hydroamination of alkenes is highly difficult compared to that of alkynes because of the lower electron density of C=C bonds than C≡C bonds.[18] It is to be noted that there is no example of heterogeneous catalysts for alkene hydroamination. Supported Pd-complex catalysts were successfully prepared on SiO_2, Al_2O_3, and TiO_2 surfaces in a

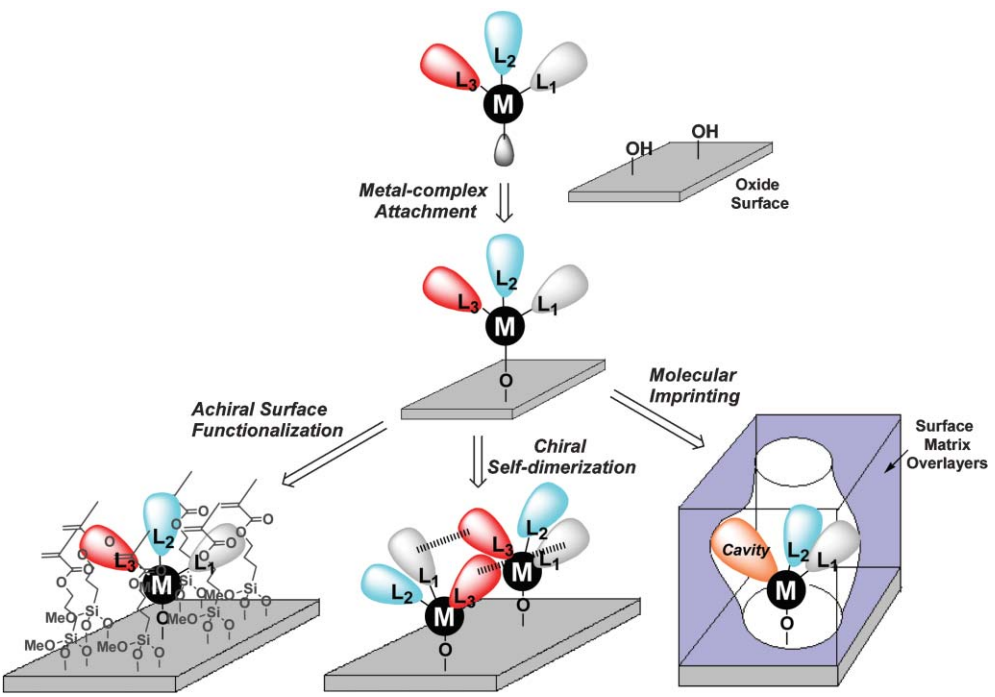

Fig. 1 Methods for advanced surface design with supported metal complexes.

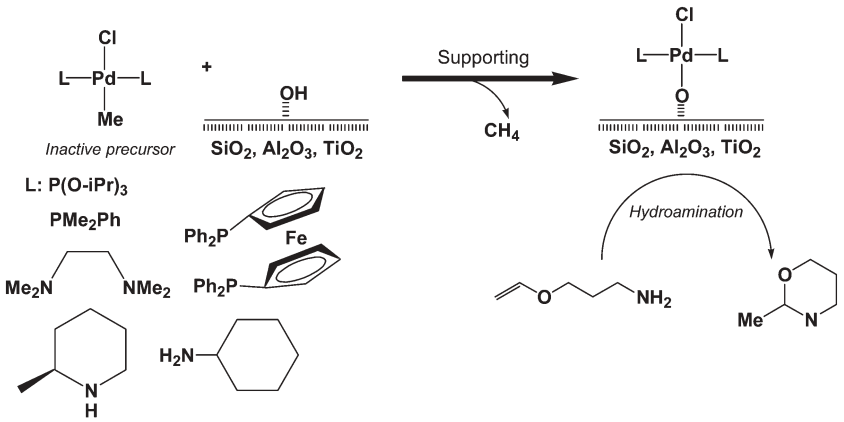

Scheme 1 Supported Pd-monomer complexes on oxide surfaces for hydroamination.

controllable manner, which are active and durable for the catalytic intrahydroamination of 3-amino-propanol vinyl ether to produce the corresponding cyclic amine.[19]

Palladium is one of the active metals for hydroamination, but its low stability to aggregation to almost inactive species under reaction conditions is one of the major problems in its use as a catalyst. Furthermore, it is known that the hydroamination activity of Pd complexes greatly depends on the nature of their anionic ligands, and hence good catalytic performance of Pd complexes is expected by chemical bonding to oxide surfaces to regulate their electronic and geometric coordination sphere. The strategy is devoted to chemical reconstruction of novel Pd–P and Pd–N complexes with a Pd–O bond formed by the chemical reaction between a methyl ligand of Pd complexes and a hydroxyl group of appropriate oxide supports.

Some new Pd monomers with Pd–P (P: $P(O–iPr)_3$, PMe_2Ph, and dppf) and Pd–N (N: tmeda, methylpiperidine, and cyclohexylamine) bonds were prepared in two or three steps. These precursors $PdMeClL_2$ were supported on SiO_2, Al_2O_3, and TiO_2 surfaces (Scheme 1), where the methyl groups quantitatively reacted with surface hydroxyl groups to evolve CH_4 in the gas phase. On the other hand, the nitrogen and phosphorus ligands of the precursors did not dissociate into the solution during the attachment reaction. A chlorine ligand remained on Pd as estimated by the intensity ratios of XPS Cl 2p and Pd 3d peaks for both the supported Pd–P and Pd–N complexes.

The XPS binding energies of Pd $3d_{5/2}$ were 336.4 eV, indicating that the Pd precursors were attached on the surfaces maintaining the oxidation state of Pd^{2+}. The curve-fitting analysis for the EXAFS Fourier-transforms at a Pd K edge for the Pd–P complexes on SiO_2 revealed the existence of a Pd–O bond at 0.212 nm (coordination number (CN) = 0.8) and Pd–P (Cl) bonds at 0.235 nm (CN = 3.1). The structures of supported Pd complexes are evidenced as Pd monomers with a Pd–O (surface) bond, a Pd–Cl bond, and two Pd–L (L: P or N) bonds (Scheme 1).[19]

Table 1 shows the catalytic activities of the hydroamination of 3-amino-propanol vinyl ether in toluene at 343 K. The homogeneous Pd precursors in toluene were completely inactive for the reaction, instead the Pd precursors decomposed. Both Pd–P and Pd–N complexes exhibited significant catalytic activities after attachment on the oxide surfaces, the intrahydroamination reactions on all the supported catalysts proceeded linearly with reaction time and the catalysts were reusable after filtration (Table 1).

There are significant differences in catalytic performance between the P and N ligands. The SiO_2-supported phosphorus-ligand complexes are more active for the reaction compared to the nitrogen-ligand complexes (Table 1). The coordination of the C=C bond of alkenes on a Pd center is an important step for the hydroamination, which is affected by the electron density of the Pd center. In the Pd–P complexes it may be regulated positively by a Pd–P orbital hybridization.

A SiO_2 support is most favorable for the Pd catalysis, while the catalytic activity on Al_2O_3 is less than one third of that on SiO_2. TiO_2 shows an intermediate support effect. The order of

Table 1 Catalytic activities (TOF: turnover frequency) of Pd-monomer precursors and oxide-supported Pd-monomer catalysts for the hydroamination of 3-amino-propanol vinyl ether[a]

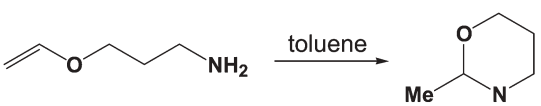

Ligand	Oxide	Pd loading/wt%[b]	TOF/h^{-1}[d]
$P(O–Pr^i)_3$	—	—	0
$PPh(CH_3)_2$	—	—	0
methylpiperidine	—	—	0
cyclohexylamine	—	—	0
$P(O–Pr^i)_3$	SiO_2	0.23	15.3
$PPh(CH_3)_2$	SiO_2	0.34	18.8
dppf	SiO_2	0.11	22.6
tmeda	SiO_2	0.44	1.1
cyclohexylamine	SiO_2	0.25	9.1
methylpiperidine	SiO_2	0.16	5.0
methylpiperidine[c]	SiO_2[c]	0.16[c]	4.8[c]
methylpiperidine	Al_2O_3	0.32	1.6
methylpiperidine	Al_2O_3	0.25	1.8
methylpiperidine[c]	Al_2O_3[c]	0.25[c]	1.7[c]
methylpiperidine	TiO_2	0.28	3.7
methylpiperidine	TiO_2	0.22	3.5
methylpiperidine[c]	TiO_2[c]	0.20[c]	3.4[c]

[a] Hydroamination of 3-amino-propanol vinyl ether was performed in toluene at 343 K under N_2. [b] Determined by XRF. [c] Reused after filtration. [d] TOF: product molecule Pd^{-1} h^{-1}.

the activities for the support is the same as that of pK_a, SiO_2 < TiO_2 < Al_2O_3. The most ionic bond, Pd–OSi, is favorable for the hydroamination of alkenes, while the Pd–OAl bond with relatively more covalent character does not efficiently promote the reaction. *These results show that the chemical bonding with surfaces is a key factor to draw out catalytic activity and appropriate surfaces can produce new catalysis.*

4. *Chiral self-assembly of metal complexes on a surface (strategy 2):* SiO_2-surface promoted chiral self-dimerization of V monomers and their asymmetric catalysis for oxidative coupling of 2-naphthol

The fine design of chirality on heterogeneous catalyst surfaces is still a serious challenge to be tackled.[20,21] However, the application of asymmetric metal complexes with chiral ligands to heterogeneous catalytic reactions is neither easy nor simple. The chemistry of homogeneous metal complexes cannot straightforwardly be transferred to chemistry on surfaces. A new strategy to construct novel chirality on surfaces which is unique to the surfaces is indispensable for the design of heterogeneous asymmetric catalysis. It is also difficult to realize both high activity and high enantioselectivity on a surface simultaneously because restriction of reaction space around the metal center to increase enantioselectivity often results in a decrease of the catalytic activity. Generally, simple immobilization of metal-complex precursors with chiral ligands on support surfaces causes commonplace catalytic performances far from the goal for asymmetric catalysis.

The oxidative coupling of 2-naphthol is a representative reaction mode for a direct synthesis of 1,1′-binaphthol (BINOL) whose optically pure derivatives are regarded as versatile chiral auxiliaries and ligands in asymmetric syntheses.[22–25] Nevertheless only a few studies have been reported for the asymmetric coupling of 2-naphthols in homogeneous systems.[26–33] Recently, we have discovered chiral self-dimerization of supported vanadium complexes on a SiO_2 surface, which is a novel phenomenon of metal complexes on oxide surfaces. Two V-monomer complexes with Schiff-base ligands are spontaneously dimerized *via* a selective reaction with a surface Si–OH group and the formed V dimer has a unique chiral conformation, which is highly enantioselective for the asymmetric oxidative coupling of 2-naphthol with 96% conversion, 100% selectivity to BINOL, and 90 ee%. To our knowledge, this is the first heterogeneous catalyst for the asymmetric coupling reaction though the V monomer is inactive for the oxidative coupling.[10,11]

Several V-monomer precursors with a Schiff-base obtained from α-amino acids (L-valine, L-isoleucine, L-leucine, L-*tert*-leucine, and L-phenylalanine) (Scheme 2) were synthesized and the attachment of the precursors on oxide surfaces was performed by impregnation of each V complex in dehydrated ethanol, followed by evacuation of the solvent under vacuum. The V monomers selectively reacted with surface silanols leading to the structural reconstruction of the tridentate Schiff-ligand coordination, as characterized by FT-IR, ESR, XAFS, XPS, XRF, UV/VIS, and DFT calculations at each stage during the attachment of the V complex precursor and the oxidative coupling of 2-naphthol. The Ph–O moiety of the Schiff-base ligand was selectively transformed to Ph–OH configuration *via* a surface reaction with surface Si–OH, resulting in a coordinatively unsaturated V conformation on the SiO_2 surface (Scheme 2).[10,11]

The pre-edge position of the V K-edge XANES spectrum (Fig. 2 (A)) and the XPS V 2p binding energy reveal that V valence in the supported V complex stays at 4+, the same as that of the V precursor. Upon attachment to the support a V=O bond was preserved, but the symmetry of the V complexes became distorted as monitored by the appearance of a d–d transition in DR-UV/VIS spectra. These behaviors were observed independent of the amount of V loading. Curve-fitting analysis of the V K-edge EXAFS spectra (Fig. 2 (B)) revealed the local structure of the attached V complex as an unsaturated conformation different from that of the V-monomer precursor. There are two kinds of chemical

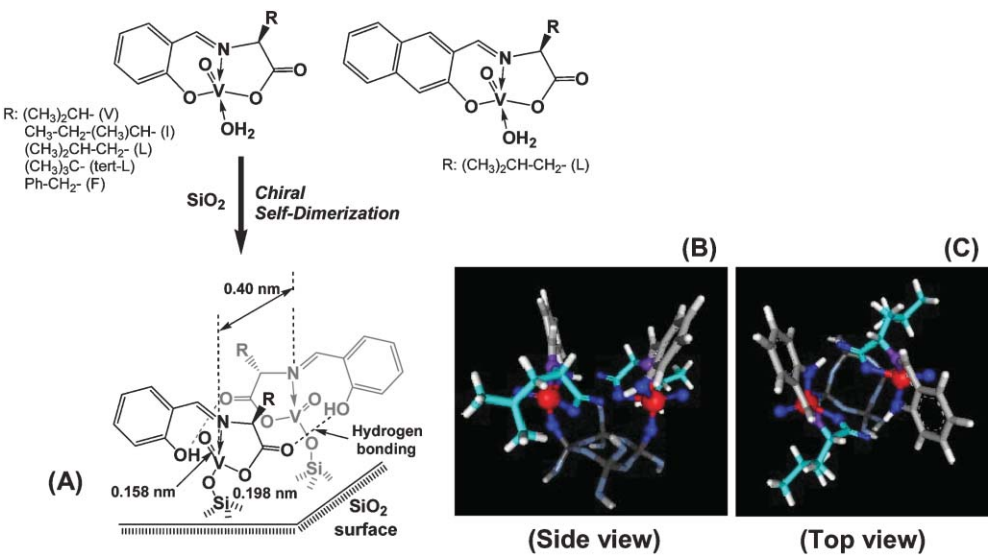

Scheme 2 Chiral self-dimerized V complex on SiO_2 (A) and its DFT modeled structures ((B) side view and (C) top view).

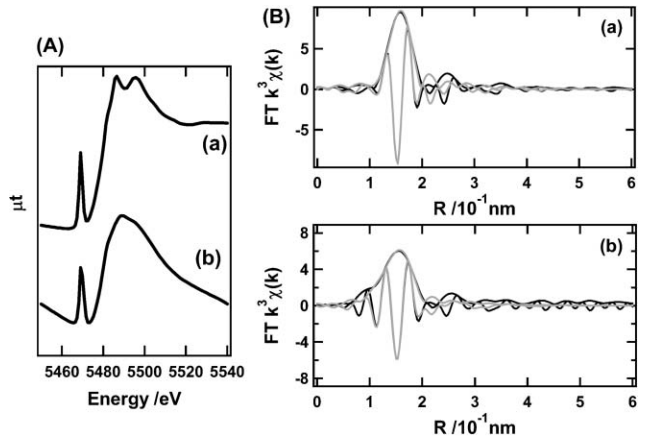

Fig. 2 V K-edge (A) XANES spectra and (B) EXAFS Fourier transforms for (a) a V precursor (L-leucine) and (b) its SiO_2-supported V complex (V 3.4 wt%). Black and gray lines represent observed and fitted spectra, respectively.

bonding of a V=O bond at 0.157 ± 0.001 nm, which is similar to that of the precursor, while the CN of V–O bonds at 0.199 ± 0.002 nm decreased from 3.8 ± 0.4 to 2.8 ± 0.5 after the attachment on the SiO_2 surface. The decrease in the CN of V–O on attachment to the support was also observed for 0.8, 1.6, and 3.4 V wt% samples independent of V loading. Longer-distance bonding was not observed with all the catalysts, indicating that there was no direct V–V bonding in the supported V catalysts.

EXAFS and FT-IR spectra of the supported V complexes demonstrate that the unique surface-attaching reaction proceeded through surface Si–OH groups. The decrease in the coordination number of V–O(N) bonds indicates that the V center becomes unsaturated on the surface. All coordination sites of the Schiff-base ligand to the V^{4+} center possess infrared-active functional groups, Ph–O, Ph ring, C=N, and COO as shown in Scheme 2: three frequencies (1598, 1373, and 1362 cm^{-1}) are assigned as one $\nu_{asym(COO)}$ and two $\nu_{sym(COO)}$; the 1629 cm^{-1} peak is assigned to $\nu_{(C=N)}$; four peaks of 1547, 1470, 1447, and 1436 cm^{-1} are referred to $\nu_{(Ph)}$; a strong peak of 1290 cm^{-1} is attributed to $\nu_{(Ph-O)}$. A small difference between $\nu_{asym(COO)}$ and $\nu_{sym(COO)}$ ($\sim$ 230 cm^{-1}) indicates the delocalization of electron density on the C=O bond to O–CO, which forms a hydrogen bond with a Ph–OH group of an adjacent V complex as discussed hereinafter.

After the attachment on SiO_2, these vibration frequencies were observed at $\nu_{(C=N)}$ 1629 cm^{-1}, $\nu_{asym(COO)}$ 1602 cm^{-1}, $\nu_{(Ph)}$ 1554, 1548, 1471, and 1452 cm^{-1}, $\nu_{sym(COO)}$ 1370 cm^{-1}, and $\nu_{(Ph-O)}$ 1391 cm^{-1}. A difference between $\nu_{asym(COO)}$ and $\nu_{sym(COO)}$ was also small, which implies that there is hydrogen bonding on C=O, which leads to delocalization of the electron density. The $\nu_{(C=N)}$, $\nu_{asym(COO)}$, and $\nu_{sym(COO)}$ were very similar to those of the precursor, indicating no significant change in the original coordination of these groups upon attachment to the support. On the other hand, the four $\nu_{(Ph)}$ peaks were different from those of the precursor in both their positions and relative intensities and the $\nu_{(Ph-O)}$ at 1290 cm^{-1} for the precursor dramatically shifted to 1391 cm^{-1} upon attachment to the support. Such a large shift was observed on ionized molecule Ph–O^-, therefore, the large shift of $\nu_{(Ph-O)}$ and the changes in the intensity ratio of $\nu_{(Ph)}$ were caused by the structural reconstruction of the Ph–O coordination to produce a new Ph–OH moiety that was promoted by proton transfer from Si–OH. These results demonstrate that the PhO^- coordination is dispatched from the V center by the reaction of the V precursor with the Si–OH to form a Ph–OH group as illustrated in Scheme 2.[10,11]

Fig. 3 shows ESR spectra for a V–L-leucine monomer precursor and its supported complex in the presence and absence of O_2 measured at 6 K. The V-monomer precursor showed hyperfine signals attributed to d^1 configuration of a V=O complex, while a different broad peak was also observed on the hyperfine signals for the supported V complex. It greatly increased after the adsorption of O_2 and the half-band signal was also detected as shown in Fig. 3 (b). The results demonstrate that another V complex is located near a V complex to form a dimer assembly. The V–V distance in the V dimer produced by self-assembly on the surface is estimated to

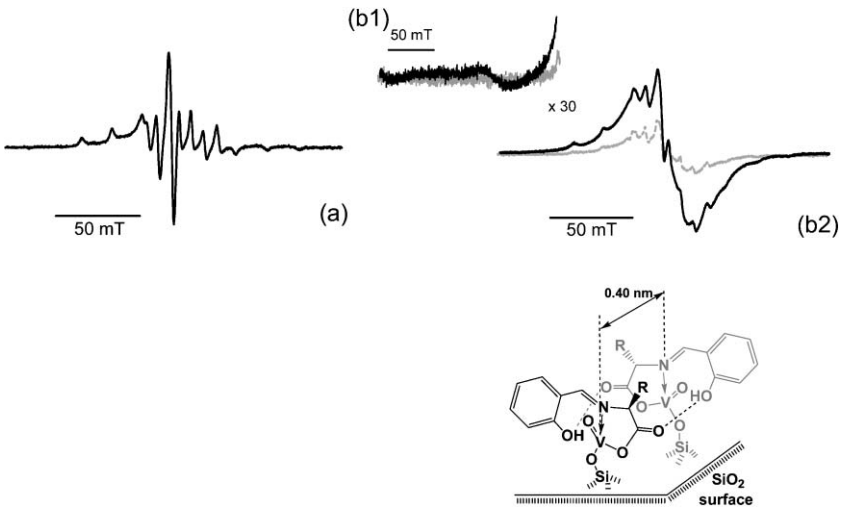

Fig. 3 ESR spectra at 6 K for a V precursor (L-leucine) in methanol (a) and the SiO_2-supported V complex (V: 3.4 wt%) in the absence (gray line) and presence (black line) of O_2 (b1: half band and b2: main signal).

be 0.40 ± 0.05 nm from the relative intensity of the forbidden half-field transition (|ΔMs| = 2) to the allowed transition (|ΔMs| = 1).[34] After evacuation of the O_2-adsorbed sample, the intensity returns completely to the original one and the change in the ESR signal occurs reversibly, which indicates the reversible adsorption of O_2 molecules on the V dimer. Thus the supported V catalyst possesses capacity for O_2 activation that is indispensable for the oxidative coupling reaction. The broad signal and the behavior for oxygen molecules were observed in the range of V loading 0.3–3.4 wt%, indicating that the chiral self-dimerization of the V precursors occurs independently of the V loading on the SiO_2 surface.

The Ph–OH moiety formed by the surface reaction of the V monomer precursor with surface OH groups forms a hydrogen bond with the C=O group of the ligand in the adjacent V complex to assemble the supported V complexes on the surface as illustrated in Scheme 2. The presence of $\nu_{asym(COO)}$ and $\nu_{sym(COO)}$ ($\Delta\nu$: 232 cm^{-1}) in the FT-IR spectrum indicates the occurrence of hydrogen bonding at the C=O oxygen, which results in the C=O and C–O bonds being coupled as $\nu_{asym(COO)}$ and $\nu_{sym(COO)}$. The V-monomer precursor selectively reacted with a surface Si–OH group, and this was followed by chiral self-dimerization to form a novel V dimer with hydrogen bonding between Ph–OH and C=O on the surface. The DFT calculation for the structure of the chiral self-dimerized V dimer on SiO_2 reveals that two V=O bonds are directed to the opposite sides mutually from the principal molecular plane of the V complex, making chiral V sites, similar to a structural unit in the V complex crystal.[35] The DFT modeling also indicates that a favorable reaction space for the oxidative coupling of two 2-naphthols in the chiral pocket is created between the two unsaturated chiral V centers (Scheme 2).

The supported V catalysts were active for the coupling of 2-naphthol under aerobic conditions, while the homogeneous V precursor is inactive for the reaction (Table 2).[10,11] On the SiO_2-supported V catalysts, the conversion reaches a maximum of 96%, and the reaction rate in toluene is 1.3 times higher than that in $CHCl_3$. The supported V catalyst is perfectly selective (100% selectivity) and reusable for the BINOL synthesis as shown in Table 2. On the other hand, Al_2O_3 and TiO_2 were not suitable as supports for the V precursor, leading to low selectivities for BINOL.

Enantioselectivity was not modified by the chiral alkyl groups of Schiff-base ligands as shown in Table 2: there are no significant differences in performance between the catalysts derived from isoleucine (51 ee%), leucine (54 ee%), and phenylalanine (56 ee%) in $CHCl_3$. The most bulky ligand, L-*tert*-leucine, has a *tert*-butyl group neighboring the V reaction site, but it reduced the enantioselectivity. These two alkyl groups overhung outside the V complexes as illustrated

Table 2 Catalytic performances of homogeneous and heterogeneous V catalysts for the oxidative coupling of 2-naphthol

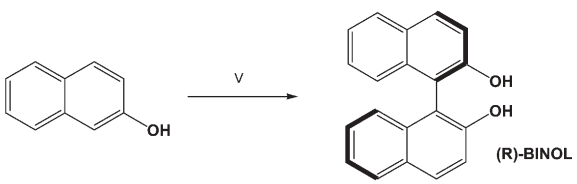

Catalyst-ligand[a,b]	Temp./K	Time/day	Solvent	Conv. (%)	Selectivity (%)	ee% (*R*)
Precursor-L[c]	293	5	$CHCl_3$	0	0	—
Precursor-L[c,d]	293	3	$CHCl_3$	15	73	8
Precursor-L[c,d]	263	9	$CHCl_3$	0	0	—
V–L/SiO_2 0.3 wt%	293	5	$CHCl_3$	76	100	19
V–L/SiO_2 0.3 wt%	263	5	$CHCl_3$	9	100	54
V–L/SiO_2 0.3 wt%	293	5	toluene	96	100	13
V–L/Al_2O_3 1.7 wt%	293	5	$CHCl_3$	69	53	−2
V–L/TiO_2 0.8 wt%	293	5	$CHCl_3$	52	0	—
V–V/SiO_2 0.3 wt%	293	2	$CHCl_3$	26	100	12
V–V/SiO_2 0.3 wt%	293	5	toluene	99	100	5
V–V/SiO_2 0.3 wt%	263	6	toluene	12	100	14
V–I/SiO_2 0.3 wt%	293	3	$CHCl_3$	37	100	17
V–I/SiO_2 0.3 wt%	263	5	$CHCl_3$	6	100	51
V–I/SiO_2 0.3 wt%	293	2	toluene	41	100	21
V–L/SiO_2 0.3 wt%[e]	293	2	toluene	40	100	13
V–L/SiO_2 0.3 wt%[e]	263	6	toluene	9	100	31
V-*tert*-L/SiO_2 0.3 wt%	263	5	toluene	11	100	12
V–F/SiO_2 0.3 wt%	293	5	$CHCl_3$	81	100	10
V–F/SiO_2 0.3 wt%	263	5	$CHCl_3$	9	100	56
V–L/SiO_2 0.3 wt%	263	5	toluene	11	100	32
V–L/SiO_2 0.3 wt%[f]	263	5	toluene	10	100	33
V–L/SiO_2 0.8 wt%	263	5	toluene	33	100	39
V–L/SiO_2 1.6 wt%	263	5	toluene	42	100	48
V–L/SiO_2 3.4 wt%	263	5	toluene	93	100	90
V–L/SiO_2 3.4 wt%[f]	263	5	toluene	91	100	89

[a] V dimer/2-naphthol was 1/36 and 100 mg of supported catalysts were used in 5 ml of toluene. [b] L: L-leucine, V: L-valine, I: L-isoleucine, *tert*-L: L-*tert*-leucine, and F: L-phenylalanine. [c] Homogeneous reaction. [d] Chlorotrimethylsilane was added as acid. [e] Hydroxy naphthaldehyde was coordinated instead of salicylaldehyde. [f] Reused.

in Scheme 2, and seemingly they did not affect the asymmetric coupling of 2-naphthol.

V loading on SiO_2 including a L-leucine segment was varied in the V loading range 0.3–3.4 wt% in order to maximize enantioselectivity for the coupling reaction (Table 2). No leaching of V complexes was observed for all the supported catalysts in toluene. Accompanying an increase in V loading to 0.3, 0.8, 1.6, and 3.4 wt%, the enantioselectivity dramatically increased: 32, 39, 48, and 90 ee%, respectively, as shown in Table 2. The 3.4 wt% V catalyst corresponding to full coverage of the V complex exhibited 90 ee%, which is comparable to the best performance for the coupling of 2-naphthol on a homogeneous catalyst reported thus far.[30–33] Furthermore, the supported V catalysts can be reused after filtration and exhibited similar catalytic performances as shown in Table 2. From the estimation of the cross section of the V precursor, the V loading of 3.4 wt% corresponds to a full coverage of the complex on the SiO_2 surface, where the configuration and reaction environment of the V dimer on the surface are regulated rigidly for the achievement of the high enantioselectivity compared to the lower V loadings.

Reaction rate (TOF) under O_2 was 3.6 day^{-1}. On the other hand, when N_2 was admitted to the same reaction system after evacuation of O_2, TOF was as low as 0.24 day^{-1}. The reaction completely stopped and no further BINOL was produced in a prolonged reaction. This limited amount of produced BINOL under N_2 may be due to the residual O_2 remaining after the O_2 evacuation. The admission of O_2 to the reaction system recovered the initial catalytic activity of 3.7 day^{-1}. Hence the presence of O_2 is a prerequisite for the oxidative coupling of 2-naphthol. The activation energies, activation enthalpies and activation entropies were 47 kJ mol^{-1}, 45 kJ mol^{-1} and -144 J K^{-1} mol^{-1}, respectively in toluene and 49 kJ mol^{-1}, 47 kJ mol^{-1} and -140 J K^{-1} mol^{-1}, respectively in $CHCl_3$. There was no significant solvent effect on these kinetic parameters.[11]

It is noteworthy that the enantioselectivity of the coupling reaction is determined by the chiral conformation on the V center rather than the chirality of the Schiff-base ligands. The chirality of the ligands affects sterically the chiral self-dimerization of V complexes on the surface, and the chiral ligands themselves do not determine the enantioselectivity for the 2-naphthol coupling. The increase in V loading on SiO_2 achieved higher regulation of the mobility of the assembled V species on the surfaces, resulting in the high enantio excess of 90 ee% at 93% conversion on the V 3.4 wt% catalyst compared to the case of the V 0.3 wt% catalyst with the same V structure (Table 2). This is the first heterogeneous catalyst with active self-assembly structure for the asymmetric oxidative coupling of 2-naphthol. *The phenomenon and the concept of the self-assembly of metal complexes on surfaces provide a new promising way to produce active species for a variety of heterogeneous enantioselective catalyses*.

5. *Surface functionalization (strategy 3):* Enantioselective Diels–Alder reaction promoted by achiral reagents on a surface

BOX (bis(oxazoline)) is one of the practical ligands for asymmetric catalysis[36–40] and several heterogeneous Cu–BOX systems have been reported.[41–46] We have found that the surface functionalization of SiO_2 with achiral 3-methacryloxypropyl-trimethoxysilane remarkably amplifies the enantioselective catalysis of SiO_2-supported Cu–BOX complexes for asymmetric Diels–Alder reaction. Enantioselectivity for Diels–Alder reaction can be significantly regulated by surface functionalization with achiral silane-coupling reagents on SiO_2-supported Cu–BOX complexes.[6,15]

The SiO_2-supported Cu–BOX catalysts were prepared in a controllable manner (Scheme 3). A BOX ligand was grafted on a SiO_2 surface and the surface around the immobilized BOX ligand was covered with several silane-coupling reagents ((a): *p*-styryltrimethoxysilane; (b): 3-phenylaminopropyltrimethoxysilane; (c): ureidopropyltriethoxysilane; (d): trimethoxyvinylsilane; (e): 3-glycidoxypropyltrimethoxysilane; (f): 3-(2-aminoethylaminopropyl)trimethoxysilane; (g): octyltriethoxysilane; (h): octadecyltriethoxysilane; (i): 3-methacryloxypropyltrimethoxysilane). $Cu(ClO_4)_2{\cdot}6H_2O$ was coordinated to the BOX ligand on the surface both with/without the functionalizing reagents (Scheme 3). The immobilization of the BOX ligand and the silane coupling reagents was confirmed by ^{29}Si solid-state MAS NMR, and the amount of the supported BOX ligand was estimated to be 0.03 mmol g^{-1} (0.1 BOX molecule nm^{-2}) by δ_{C-H} peak intensity at 1370 cm^{-1} in FT-IR.

The ESR signal of a supported Cu–BOX complex ($g_{//}$ = 2.291, $A_{//}$ = 12.6, and $g_{\perp}$ = 2.083) was observed at higher magnetic fields than that of the $Cu(ClO_4)_2$ precursor, which demonstrates that the precursor was coordinated to the immobilized BOX ligand because the ESR signals for Cu^{2+} species coordinated by nitrogen ligands were observed at higher magnetic fields.[47] A peak observed around 370 nm for the supported Cu–BOX catalyst in diffuse-reflectance UV/VIS spectra indicated similar local structure to a homogeneous analog $Cu(BOX)(ClO_4)_2$. The bond distance and total coordination number (CN) of Cu–O (Cu–N) in the supported Cu–BOX catalyst were 0.199 $\pm$ 0.001 nm and 4.4 $\pm$ 0.5, respectively by Cu K-edge EXAFS, which were almost the same as 0.198 $\pm$ 0.001 nm and 4.5 $\pm$ 0.6 for $Cu(BOX)(ClO_4)_2$. Similar structural parameters were also observed for the surface-functionalized Cu–BOX catalysts, indicating that the local structures of both Cu–BOX complexes on the SiO_2 surface were the same as $Cu(BOX)(ClO_4)_2$ as shown in Scheme 3.[15]

In spite of the similar local coordination of the Cu–BOX complexes, the catalytic performances for the Diels–Alder reaction of cyclopentadiene and 3-acryloyl-2-oxazolidinone (Table 3) were tremendously different from each other. The homogeneous Cu–BOX complex showed a low enantioselectivity of 5 ee% (*S*) at concentrations of both 25 and 0.35 mmol l^{-1} of the Cu complex. The catalytic activity of the homogeneous Cu–BOX complex, particularly at the low concentration, was very low (conversion: 4% after 1 h). On the other hand, the catalytic reaction proceeded on the simple supported Cu–BOX catalyst without surface functionalization and was complete after 24 h as shown in Table 3.

Interestingly, the surface functionalization remarkably changed the enantioselectivity although the surface building

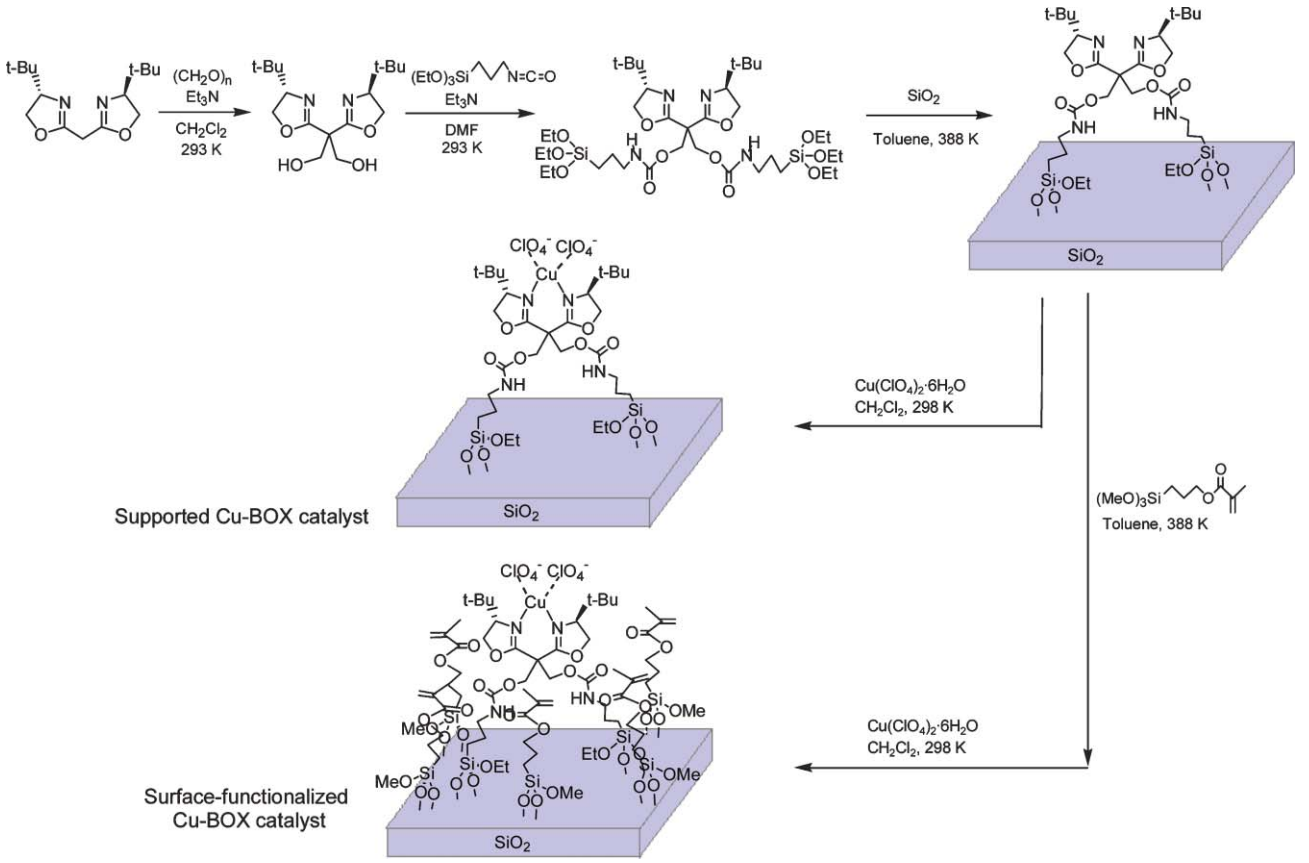

Scheme 3 Preparation of surface-functionalized Cu–BOX complexes on SiO_2.

blocks are not optically active. Especially, in the case of (i) 3-methacryloxypropyltrimethoxysilane, the surface-functionalized catalyst brought about a large increase in the enantioselectivity as shown in Table 3. The enantioselectivity highly depended on the kinds and amounts of the functionalized reagents and it was found that further surface-functionalization up to a full coverage of the achiral (i), 0.6 mmol g^{-1}, increased the enantioselectivity to 65 ee% of endo conformation product. After 24 h, the conversion reached 100%, while keeping a similar enantioselectivity (63 ee% of endo) (Table 3). The silane-coupling reagent (i) without attachment on SiO_2 was added to the CH_2Cl_2 solution in which the simple immobilized Cu–BOX catalyst was suspended, but no increase in the enantioselectivity was observed. Thus the chemical bonding of (i) to the surface may be indispensable for the promotion of enantioselective catalysis, and the full-coverage functionalization with (i) is most effective for the creation of an enantioselective reaction field on the surface. The functionalized Cu–BOX catalyst was reusable without significant loss of the catalytic activity (88% conversion at 24 h) and the enantioselectivity (58 ee% of endo) as shown in Table 3.

Other silane-coupling reagents with styryl (a) and vinyl (d) groups cause large decreases in the enantioselectivity (Table 3). It has been reported that the capping of free surface Si–OH with trimethylsilyl moieties is favorable for asymmetric catalysis on SiO_2.[45,48] However, the results for (a) and (d) indicate that the capping of silanol groups does not lead to an increase in the enantioselectivity. Long alkyl chains such as octyl (g) and octadecyl (h) groups influenced ee% a little. Ee% for the longer octadecyl group (h) (25 ee%) was higher than the 13 ee% for the shorter octyl group (g), while the catalytic activities were similar to each other. Phenylamino (b), urea (c), epoxy (e), and amino (f) brought about a large loss of the catalytic activities because these reagents act as bidentate ligands for Cu^{2+} to probably decompose the original Cu–BOX complex.

Only the methacryl-functionalized catalyst (i) showed high enantioselectivity for the Diels–Alder reaction. As the lengths of methacryl reagent (i) and the BOX ligand on SiO_2 are similar to each other, the oxygen of the methacryl group may interact with the NH group of the chiral BOX ligand by hydrogen bonding. The dependence of the enantioselectivity on the coverage of (i) indicates that the achiral methacryl groups surround the supported chiral BOX ligand to form a new assembled structure of the chiral BOX with the achiral methacryl groups, resulting in the large increase in the ee%. The values of ee%s in polar $CHCl_3$ and ethanol were as small as 0.8 and 5 ee%, respectively, also agreeing with the assumption of the assembled structure on the surface. This gluing effect of achiral methacryl groups on the chiral BOX ligand may be the origin of the increase in the chiral selectivity. *The present results demonstrate that the non-chiral design of catalyst surfaces has the potential to create novel asymmetric reaction fields that are unique on the surfaces.*

Table 3 Asymmetric Diels–Alder reactions of cyclopentadiene and 3-acryloyl-2-oxazolidinone catalyzed on homogeneous $Cu(ClO_4)_2$–BOX, simple supported catalyst and surface-functionalized Cu–BOX catalysts at 263 K

Catalyst	Solvent	Time/h	Conv. (%)	endo%	ee% (*S*) (endo)
Homogeneous					
$Cu(ClO_4)_2$–BOX	CH_2Cl_2	1	4	89	5
$Cu(ClO_4)_2$–BOX[a]	CH_2Cl_2	3	98	89	5
Simple supported					
	CH_2Cl_2	1	61	90	15
		24	100		14
With i[b]	CH_2Cl_2	1	58	90	15
Functionalized					
i: methacryl[c]	CH_2Cl_2	1	12	91	49
		24	100		42
i: methacryl[d]	CH_2Cl_2	1	16	93	65
		24	100		63
i: methacryl[d,e]	CH_2Cl_2	24	88	93	58
i: methacryl[d]	toluene	24	100	91	38
i: methacryl[d]	$CHCl_3$	24	88	92	0.8
i: methacryl[d]	ethanol	24	86	90	5
a: styryl[d]	CH_2Cl_2	1	5.3	97	0
b: phenylamino[d]	CH_2Cl_2	1	0.4	90	1
c: urea[d]	CH_2Cl_2	1	1.2	90	2
d: vinyl[d]	CH_2Cl_2	1	33	90	3
e: epoxy[d]	CH_2Cl_2	1	0.3	88	6
f: diamine[d]	CH_2Cl_2	1	0.2	91	11
g: octyl[d]	CH_2Cl_2	1	11	96	13
h: octadecyl[d]	CH_2Cl_2	1	11	89	25

[a] Concentration of Cu was 25 mmol l^{-1}. [b] 3-Methacryloxypropyltrimethoxysilane (i) was added to the solution. [c] Loading of (i) was 1 nm^{-2}. [d] Loading of (i) was 2 nm^{-2}. [e] Reused.

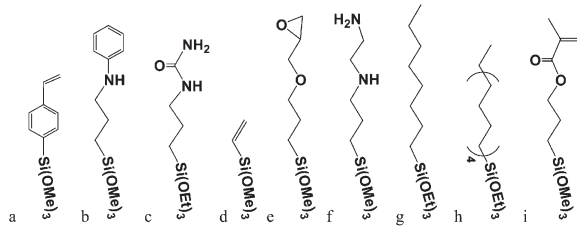

[f] Ratio of Cu/diene/dienophile = 1/40/10. Concentration of Cu was 0.35 mmol l^{-1}.

6. *Molecular imprinting (strategy 4):* Molecular-imprinted catalysts designed at oxide surfaces

To prepare artificial enzymatic systems possessing recognition ability for particular substrate molecules, molecular imprinting methods which create template-shaped cavities with memory of template molecules in polymer matrices have been developed and established in receptors, chromatographic separations, fine chemical sensing, *etc.* in the past decade.[49–54] Nevertheless, artificial enzymatic materials synthesized by molecular imprinting techniques using a variety of template molecules provide promising molecular recognition catalysis with 100% selectivity for a variety of catalytic reactions where natural enzymes cannot be employed. Recently, in addition to imprinted acid–base catalysts,[55–61] attempts to imprint metal complexes have been reported and constitute state of the art currently.[6–8] Molecular imprinting of metal complexes enables the realization of several features to note, (1) attachment of a metal complex on robust supports, (2) surrounding of the metal complex by a polymer matrix, and (3) production of a shape selective cavity on the metal site in the matrix. Metal complexes thus imprinted have been applied to molecular recognition,[62,63] stabilization of a reactive complex,[64,65] ligand exchange reaction,[66] and catalysis.[67–76]

Most of the imprinted metal-complex catalysts have been prepared by imprinting in bulk polymer, while the access of substrate molecules to the sites in the bulk is disadvantageous. Such organic polymers tend not to be durable in organic solvents or under severe catalytic conditions such as in the presence of oxidants, at high temperatures, *etc*. *We have proposed the design of molecular-imprinted catalysts for oxide-supported metal complexes to produce shape-selective reaction sites for desired molecules by using a ligand on a metal center as a template*. Here we summarize our recent work on molecular imprinting metal-complex catalysts, which show remarkable catalytic performances beyond simply supported metal-complex catalysts.

A ligand of a supported metal complex not only influences its catalytic activity but also provides an unsaturated, reactive metal site with a ligand-shaped space by removal of a ligand. We chose a ligand of the attached metal complex with a similar shape to a reaction intermediate (half-hydrogenated alkyl) of alkene hydrogenation as a template molecule. Our strategy to design active and selective catalysts was based on the following five factors for regulation, (1) conformation of ligands coordinated to Rh atom, (2) orientation of vacant site on Rh, (3) cavity with the template molecular shape for reaction space produced behind template removal, (4) architecture of the cavity wall, and (5) micropore in inorganic polymer-matrix overlayers stabilizing the active species at the surface.[6,8]

Scheme 4 shows the preparation steps for molecular-imprinted Rh-monomer and Rh-dimer catalysts on SiO_2 for hydrogenation of alkenes.[73–76] Both catalysts were prepared step-by-step, characterizing their structures on the surfaces. A $P(OCH_3)_3$ ligand was used as a template with a similar shape to one of the half-hydrogenated species of 3-ethyl-2-pentene, which can produce the template (reaction intermediate)-shaped cavity by extraction of the ligand. We succeeded in preparing Rh monomer and a pair of Rh monomers by using appropriate precursors on the surfaces (Scheme 4).

On both surfaces, $Si(OCH_3)_4$ was deposited by chemical vapor deposition and hydrolysis–polymerization was conducted to prepare SiO_2-matrix overlayers surrounding the attached Rh complexes. Finally the template $P(OCH_3)_3$ ligand was extracted from the attached Rh complex in the SiO_2-matrix overlayers and the molecular imprinted Rh-monomer and Rh-dimer catalysts were successfully obtained. The peak intensity of Rh3d XPS decreased after the stacking of the SiO_2-matrix overlayers as shown in Fig. 4, demonstrating that the attached Rh complexes were embedded in the surface matrix.

Table 4 shows steady-state reaction rates (turnover frequencies (TOF)) of the hydrogenation of seven alkenes at 348 K on the supported Rh-complex catalyst and the molecular-imprinted Rh-dimer catalyst. The homogeneous complexes $Rh_2Cl_2(CO)_4$ and $RhCl(P(OCH_3)_3)_3$ and the supported species $Rh_2Cl_2(CO)_4/SiO_2$ show no activities for the reaction. On the other hand, the molecular-imprinted catalysts exhibited significant catalytic activities under similar reaction conditions. It is to be noted that the hydrogenation

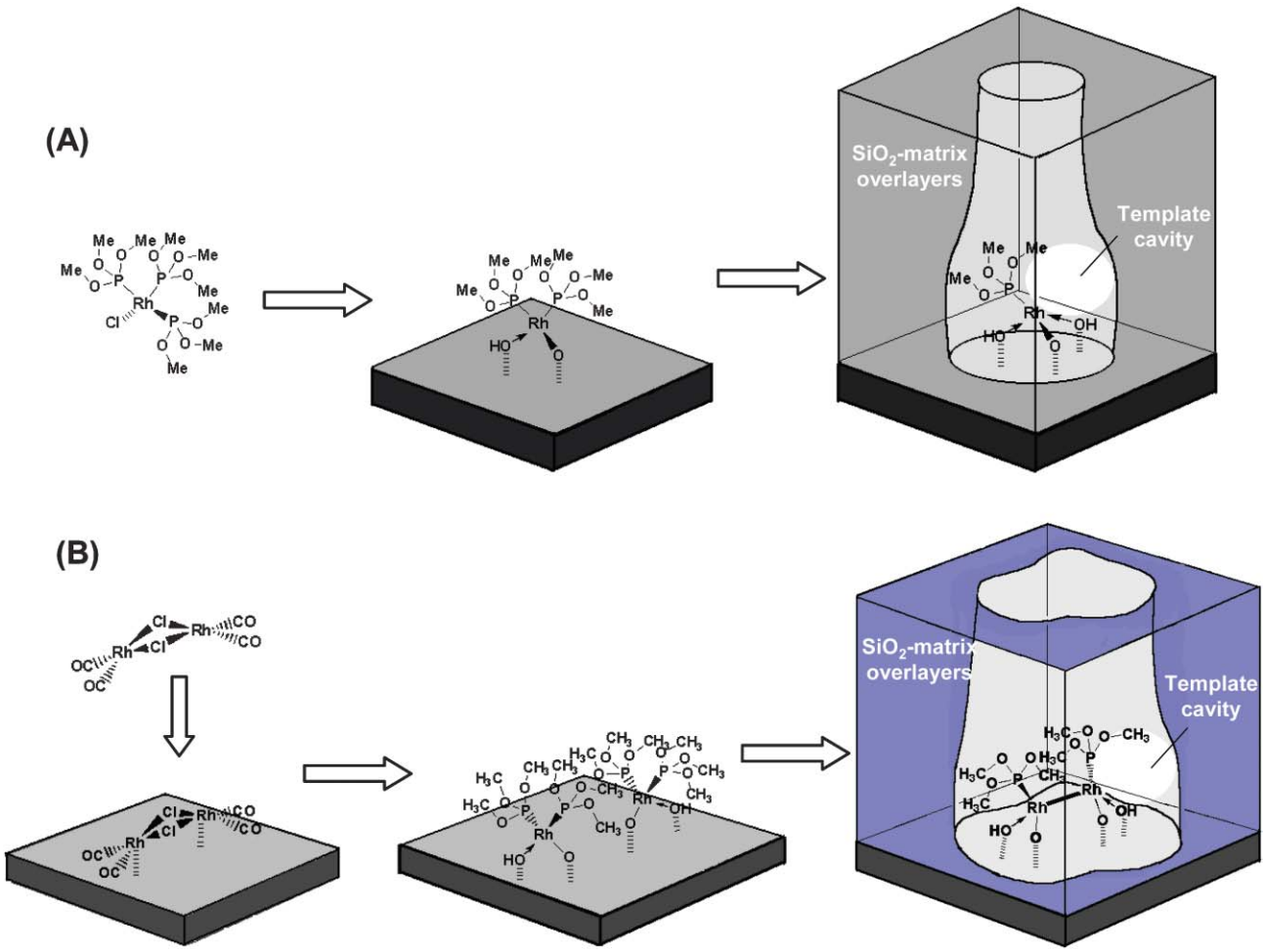

Scheme 4 Molecular imprinting of SiO_2-attached (A) Rh-monomer and (B) Rh-dimer catalysts with $P(OCH_3)_3$ ligands.

reactions are remarkably promoted by the surface imprinting. For example, hydrogenation of 2-pentene on the molecular-imprinted Rh-dimer catalyst is promoted 51 times as compared to that on the supported catalyst. The metal–metal bonding and coordinative unsaturation of the Rh dimer are key factors for the remarkable activity of the imprinted Rh-dimer catalyst. The imprinted Rh monomer after the removal of the template ligand is also relatively unsaturated, resulting in an increase in hydrogenation activity compared to the precursor complex and the simple supported catalyst.[75]

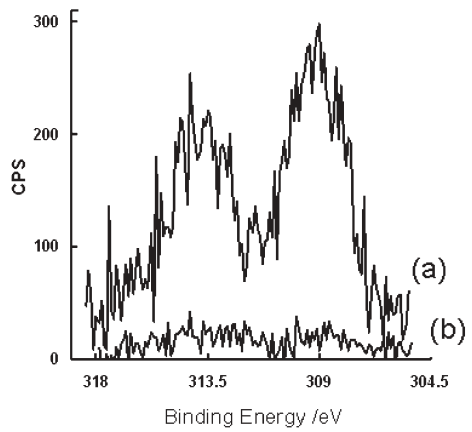

Fig. 4 Rh3d XPS spectra for (a) the supported Rh–$P(OCH_3)_3$ catalyst and (b) the molecular-imprinted Rh-dimer catalyst with SiO_2-matrix overlayers.

Ratios of TOFs corresponding to the degree of enhancement of the reaction rates by the imprinting revealed that the molecular-imprinted Rh catalysts showed size- and shape-selectivities for the alkenes as shown in Table 4. Selectivity for the alkene hydrogenation on the molecular-imprinted catalysts depended highly on the size and shape of alkenes which should come into the template cavity as a reaction site in the micropores of the SiO_2-matrix overlayers on the surfaces in addition to the electronic and geometric effects of the ligands. The TOF ratios were reduced with gain of alkene size. It is to be noted that there is a large difference in the reaction rates between 3-ethyl-2-pentene and 4-methyl-2-hexene (4-ethyl-2-pentene) due to the difference in the shape of the alkenes. The difference in the TOF ratio between 4-methyl-2-pentene and 4-methyl-2-hexene is also large, where the difference in the size of a methyl group is discriminated on the molecular-imprinted catalyst. The TOF ratio for 4-methyl-2-hexene is much smaller than that for 2-pentene, where the difference is referred to the ethyl group. Thus, the molecular-imprinted catalyst

Table 4 Degrees of enhancement of the reaction rates on the Rh-dimer catalysts by molecular imprinting (ratio of TOFs), activation energies (E_a), and activation entropies ($\Delta^{\ddagger}S$) for the catalytic hydrogenation of alkenes at 348 K

Reactant	Supported TOF/s^{-1}	Imprinted TOF/s^{-1}	Ratio of TOFs[a]	Supported		Imprinted	
				E_a[b]	$\Delta^{\ddagger}S$[c]	E_a[b]	$\Delta^{\ddagger}S$[c]
(1) 2-pentene	1.3×10^{-3}	6.6×10^{-2}	51	34	−205	26	−195
(2) 3-methyl-2-pentene	7.0×10^{-5}	3.6×10^{-3}	51	44	−200	43	−170
(3) 4-methyl-2-pentene	1.3×10^{-4}	5.9×10^{-3}	45	40	−207	40	−175
(4) 3-ethyl-2-pentene	4.4×10^{-5}	1.5×10^{-3}	35	42	−210	39	−189
(5) 4-methyl-2-hexene	6.8×10^{-5}	9.6×10^{-4}	14	40	−212	10	−276
(6) 2-octene	3.0×10^{-3}	3.0×10^{-2}	10	28	−215	7	−257
(7) 1-phenyl-propene	2.8×10^{-3}	2.0×10^{-2}	7	29	−213	8	−256

[a] Ratio of TOFs: TOF of the imprinted Rh-dimer catalyst/TOF of the supported catalyst. [b] E_a: kJ mol^{-1}. [c] $\Delta^{\ddagger}S$: J K^{-1} mol^{-1}.

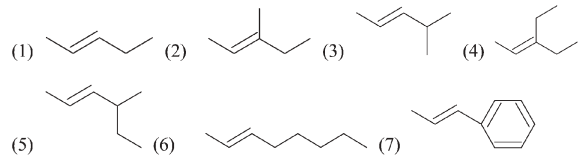

discriminates the size and shape of the alkenes. However, the molecular-imprinted catalyst cannot discriminate between the existence of methyl and ethyl groups among the alkenes smaller than the template size as shown in Table 4. It is noteworthy that the reaction rates of 2-pentene, 2-octene, and 1-phenylpropene on the simple supported catalyst are similar to each other, whereas the rate enhancements (TOF ratios) for 2-octene and 1-phenylpropene (10 and 7 times, respectively) are much less than that for 2-pentene (51 times). Because the length of the linear alkene chains cannot be discerned by the ligand-coordinated metal site, it is suggested that the difference is caused by a wall of the template cavity around the Rh dimer site.

Activation energies for the hydrogenation on the supported catalyst are divided into two values, about 30 and 42 kJ mol^{-1}, for the linear alkenes and the branched alkenes, respectively, in Table 4 and activation entropies are similar to each other, with values in the range −200 to −215 J mol^{-1} K^{-1} for all the alkenes. After the imprinting, significant differences between small and large alkenes were observed in both activation energies and activation entropies. The activation energies for the hydrogenation of 3-ethyl-2-pentene and smaller alkenes on the imprinted catalyst were 26–43 kJ mol^{-1}, which are similar to the values observed on the supported catalyst. The activation entropies for the four alkenes were −170 to −195 J mol^{-1} K^{-1} on the molecular-imprinted Rh-dimer catalyst, which are larger than those (−200 to −210 J mol^{-1} K^{-1}) obtained for the supported catalyst. In contrast, for the larger alkenes such as 4-methyl-2-hexene, 2-octene, and 1-phenylpropene, the activation energies were 10, 7, and 8 kJ mol^{-1}, respectively, which are very small compared with those for the supported catalyst and other metal complex catalysts. Furthermore, the activation entropies were reduced markedly from about −210 J mol^{-1} K^{-1} to about −260 J mol^{-1} K^{-1}. The conspicuous change in the kinetic parameters for the larger alkenes is paralleled by the change in enhancement of the reaction rates.

These dramatic decreases in the activation energies and the TOF ratios can be explained by a shift of the rate-determining step from the alkyl formation to the coordination of alkene to the Rh site. Attending this shift, the activation entropies for the larger alkene molecules also decreased markedly to about −260 J mol^{-1} K^{-1} from about −180 J mol^{-1} K^{-1} for the other small molecules. It suggests that the conformation of the coordinated alkene in the template cavity is regulated by a wall of the cavity and the remaining $P(OCH_3)_3$ ligands. For the alkenes with the larger sizes and different shapes compared to the template, the coordination to the Rh site through the cavity space becomes most slow in the reaction sequences.

The location of the Rh center to which the alkenes coordinate, the conformation of the remaining $P(OCH_3)_3$ ligand, the orientation of the template vacant site on Rh, the template-shaped cavity, the architecture of the cavity wall, and the micropore surrounding the Rh dimer in the SiO_2-matrix overlayers provide the active imprinted catalysts for size- and shape-selective hydrogenation of the alkenes. *The method combining metal-complex attachment and molecular imprinting on the surface demonstrates that the strategy can regulate and design chemical reactions at a molecular level like artificial enzyme catalysts.*

7. Conclusions

Our recent work on chemical design of catalytically active metal complexes supported on oxide surfaces was reviewed, describing the strategy and concept for the catalyst surface design. Supported metal complexes often exhibit unique catalytic performances different from metal and metal oxides for various chemical processes including shape-selective catalysis and asymmetric catalysis. Step-by-step chemical transformations of metal complexes in a controllable manner create selective reaction sites on surfaces and the fine design of space surrounding attached metal complexes is also indispensable for better achievement of selective catalysis on surfaces. Further, the arrangement of active sites on surfaces by chiral self-dimerization, surface functionalization with achiral reagents, and molecular imprinting provide new powerful ways to design catalyst surfaces and selective catalysis beyond conventional homogeneous and heterogeneous catalyst systems.

Notes and references

1 Y. Iwasawa, ed., *Tailored Metal Catalysts*, Reidel, Dordrecht, 1986.
2 Y. Iwasawa, Chemical Design for Active Surfaces, *Adv. Catal.*, 1987, **35**, 187.
3 Y. Iwasawa, *Catal. Today*, 1993, **18**, 21.
4 Y. Iwasawa, *Stud. Surf. Sci. Catal.*, 1996, **101**, 21.
5 Y. Iwasawa, *Acc. Chem. Res.*, 1997, **30**, 103.
6 M. Tada and Y. Iwasawa, *J. Mol. Catal. A: Chem.*, 2003, **199**, 115.
7 M. Tada and Y. Iwasawa, *J. Mol. Catal. A: Chem.*, 2003, **204–205**, 27.
8 M. Tada and Y. Iwasawa, *Annu. Rev. Mater. Res.*, 2005, **35**, 397.
9 Y. Iwasawa, *J. Catal.*, 2003, **216**, 165.
10 M. Tada, T. Taniike, L. M. Kantam and Y. Iwasawa, *Chem. Commun.*, 2004, 2542.
11 M. Tada, N. Kojima, Y. Izumi, T. Taniike and Y. Iwasawa, *J. Phys. Chem. B*, 2005, **109**, 9905.
12 M. Tada, S. Tanaka and Y. Iwasawa, *Chem. Lett.*, 2005, **34**, 1362.
13 S. Tanaka, M. Tada and Y. Iwasawa, in preparation.
14 R. Psaro and S. Recchia, *Catal. Today*, 1998, **41**, 139.
15 B. C. Gates, *Top. Catal.*, 2001, **14**, 173.
16 A. Zecchina and C. O. Arean, *Catal. Rev. Sci. Eng.*, 1993, **35**, 261.
17 D. Steinborn and R. Z. Taube, *J. Mol. Catal.*, 1989, **49**, 235.
18 T. Muller and M. Beller, *Chem. Rev.*, 1998, **98**, 675.
19 M. Tada, M. Shimamoto, T. Sasaki and Y. Iwasawa, *Chem. Commun.*, 2004, 2562.
20 J. M. Thomas, R. Raja and D. W. Lewis, *Angew. Chem., Int. Ed.*, 2005, **44**, 6456.
21 A. Corma, *Catal. Rev. Sci. Eng.*, 2004, **45**, 369.
22 L. Pu, *Chem. Rev.*, 1998, **98**, 2405.
23 R. Noyori, *Asymmetric Catalysis in the Organic Synthesis*, Wiley, New York, 1994.
24 Y. Chen, S. Yekta and A. K. Yudin, *Chem. Rev.*, 2003, **103**, 3155.
25 P. I. Dalko and L. Moisan, *Angew. Chem., Int. Ed.*, 2004, **43**, 5138.
26 M. Nakajima, I. Miyoshi, K. Kanayama and S. Hashimoto, *J. Org. Chem.*, 1999, **64**, 2264.
27 X. Lin, J. Yang and M. C. Kozlowski, *Org. Lett.*, 2001, **3**, 1137.
28 J. Gao, J. H. Reibenspies and A. E. Martell, *Angew. Chem., Int. Ed.*, 2003, **42**, 6008.
29 R. Irie, K. Masutani and T. Katsuki, *Synlett*, 2000, 1433.
30 C. Y. Chu, D. R. Hwang, S. K. Wang and B. J. Uang, *Chem. Commun.*, 2001, 980.
31 S. W. Hon, C. H. Li, J. H. Kuo, N. B. Barhate, Y. H. Liu, Y. Wang and C. T. Chen, *Org. Lett.*, 2001, **3**, 869.
32 Z. Luo, Q. Liu, L. Gong, X. Cui, A. Mi and Y. Jiang, *Angew. Chem., Int. Ed.*, 2002, **41**, 4532.
33 H. Somei, Y. Asano, T. Yoshida, S. Takizawa, H. Yamataka and H. Sasaki, *Tetrahedron Lett.*, 2004, **45**, 1841.
34 S. S. Eaton, K. M. More, B. M. Sawant and G. R. Eaton, *J. Am. Chem. Soc.*, 1983, **105**, 6560.
35 D. Rehder, C. Schulzke, H. Dan, C. Meinke, J. Hanss and M. Epple, *J. Inorg. Biochem.*, 2000, **80**, 115.
36 A. K. Ghosh, P. Mathivanan and J. Cappiello, *Tetrahedron: Asymmetry*, 1998, **9**, 1.
37 D. A. Evans, S. J. Miller, T. Lectka and P. von Matt, *J. Am. Chem. Soc.*, 1999, **121**, 7559.
38 J. M. Takacs, E. C. Lawson, M. J. Reno, M. A. Youngman and D. A. Quincy, *Tetrahedron: Asymmetry*, 1997, **8**, 3073.
39 A. K. Ghosh, H. Cho and J. Cappiello, *Tetrahedron: Asymmetry*, 1998, **9**, 3687.
40 J. Zhou and Y. Tang, *Org. Biomol. Chem.*, 2004, **2**, 429.
41 J. M. Fraile, J. I. García, M. A. Harmer, C. I. Herrerías and J. A. Mayoral, *J. Mol. Catal. A: Chem.*, 2001, **165**, 211.
42 P. O'Leary, N. P. Krosveld, K. P. De Jong, G. van Koten and R. J. M. Klein Gebbink, *Tetrahedron Lett.*, 2004, **45**, 3177.
43 R. Annunziata, M. Benaglia, M. Cinquini, F. Cozzi and M. Pitillo, *J. Org. Chem.*, 2001, **66**, 3160.
44 K. Hallman and C. Moberg, *Tetrahedron: Asymmetry*, 2001, **12**, 1475.
45 D. Rechavi and M. Lemaire, *J. Mol. Catal. A: Chem.*, 2002, **182–183**, 239.
46 J. K. Park, S.-W. Kim, T. Hyeon and B. M. Kim, *Tetrahedron: Asymmetry*, 2001, **12**, 2931.
47 M. Soibinet, I. D. Olivier, A. Mohamadou and M. Aplincourt, *Inorg. Chem. Commun.*, 2004, **7**, 405.
48 S. J. Bae, S.-W. Kim, T. Hyeon and B. M. Kim, *Chem. Commun.*, 2000, 31.
49 P. A. Brady and J. K. M. Sanders, *Chem. Soc. Rev.*, 1997, **26**, 327.
50 D. C. Sherrington, *Chem. Commun.*, 1998, 2275.
51 M. E. Davis, A. Katz and W. R. Ahmad, *Chem. Mater.*, 1996, **8**, 1820.
52 B. Shellergren, *Angew. Chem., Int. Ed.*, 2000, **39**, 1031.
53 M. J. Whitecombe, C. Alexander and E. N. Vulfson, *Synlett*, 2000, **6**, 911.
54 K. Mosbach, *Chem. Rev.*, 2000, **100**, 2495.
55 K. Morihara, M. Kurosawa, Y. Kamata and T. Shimada, *J. Chem. Soc., Chem. Commun.*, 1992, 358.
56 J. Heilmann and W. F. Maier, *Angew. Chem., Int. Ed. Engl.*, 1994, **33**, 471.
57 A. Katz and M. E. Davis, *Nature*, 2000, **403**, 286.
58 A. G. Strikovsky, D. Kasper, M. Crun, B. S. Green, J. Hradil and G. Wulff, *J. Am. Chem. Soc.*, 1999, **121**, 6640.
59 M. A. Markowitz, P. R. Kust, G. Deng, P. E. Schoen, J. S. Dordick, D. S. Clark and B. P. Gaber, *Langmuir*, 2000, **16**, 1759.
60 T. Tanimura, N. Katada and M. Niwa, *Langmuir*, 2000, **16**, 3858.
61 A. Suzuki, M. Tada, T. Sasaki, T. Shido and Y. Iwasawa, *J. Mol. Catal. A: Chem.*, 2002, **182–183**, 125.
62 Y. Fujii, K. Matsutani and K. Kikuchi, *J. Chem. Soc., Chem. Commun.*, 1985, 415.
63 J. Suh, Y. Cho and K. J. Lee, *J. Am. Chem. Soc.*, 1991, **113**, 4198.
64 J. F. Krebs and A. S. Borovik, *J. Am. Chem. Soc.*, 1995, **117**, 10593.
65 J. F. Krebs and A. S. Borovik, *Chem. Commun.*, 1998, 553.
66 N. M. Brunkan and M. R. Gagne, *J. Am. Chem. Soc.*, 2000, **122**, 6217.
67 J. Matsui, I. A. Nicholls, I. Karube and K. Mosbach, *J. Org. Chem.*, 1996, **61**, 5414.
68 F. Locatelli, P. Gamez and M. Lemaire, *J. Mol. Catal. A: Chem.*, 1998, **135**, 89.
69 B. P. Santora, A. O. Larsen and M. R. Gagne, *Organometallics*, 1998, **17**, 3138.
70 K. Polborn and K. Severin, *Chem.-Eur. J.*, 2000, **6**, 4604.
71 K. Polborn and K. Severin, *Eur. J. Inorg. Chem.*, 2000, 1687.
72 A. N. Cammidge, N. J. Baines and R. K. Bellingham, *Chem. Commun.*, 2001, 2588.
73 M. Tada, T. Sasaki and Y. Iwasawa, *Phys. Chem. Chem. Phys.*, 2002, **4**, 4561.
74 M. Tada, T. Sasaki, T. Shido and Y. Iwasawa, *Phys. Chem. Chem. Phys.*, 2002, **4**, 5899.
75 M. Tada, T. Sasaki and Y. Iwasawa, *J. Catal.*, 2002, **211**, 496.
76 M. Tada, T. Sasaki and Y. Iwasawa, *J. Phys. Chem. B*, 2004, **108**, 2918.